Using a Fast-Scanning Electrical Nanoparticle Sizer to Characterize Nanoparticles from Laser Ablation

Chaolong Qi[1], Da-Ren Chen[1*], Meng-Dawn Cheng[2]

[1] Environmental Engineering Science Program Washington University in St. Louis, Campus Box 1180, One Brookings Drive, St. Louis, MO 63130

[2] Environmental Science Division, Oak Ridge National Laboratory, Oak Ridge, TN 37831

Abstract

A Fast-Scanning Electrical Nanoparticle Sizer (FSENS) consisting of a Po^{210} bipolar charger, a Nano-DMA, and an aerosol electrometer was used to characterize nanoparticles generated by laser ablating the surfaces of cement, chromium-embedded cement, stainless steel, and alumina samples. Different from previous studies, bimodal size distributions, with the nucleation mode having a geometric mean diameter ranging from 5.7-6.6 nm and a geometric standard deviation varying from 1.225-1.379, were observed for all the experimental runs. The curve fitting shows that the bimodal size distribution produced in the laser ablation can be best fitted by a lognormal distribution for the nucleation mode and a Rosin-Rammler distribution for the coagulation mode. At steady state the geometric mean diameter of the coagulation mode was affected by the laser wavelength and target material, but was less influenced by laser energy for a given wavelength. The total particle number concentrations of the two modes appear to be parabolic with respect to the laser fluence. At a given fluence, the stainless-steel sample produced the highest particle number concentration with 532- and 1064-nm lasers; the alumina sample produced the lowest particle number concentration with 266- and 1064-nm lasers. The chromium-embedded cement sample produced fewer particles with 532- and 1064 nm lasers than the pure cement sample. This study also demonstrated that FSENS can provide snapshots of the nanoparticle dynamics during laser ablation in cases of low laser fluence.

***Keywords*:** Nanoparticle; Laser ablation; Nanoparticle dynamics.

[*] Corresponding author. Tel.: 1-314-935-7924, Fax: 1-314-935-5464

E-*mail address*: chen@me.wustl.edu

INTRODUCTION

Laser ablation is a process removing materials from solid target surfaces by laser irradiation. The high-power lasers remove solid materials either directly through laser vaporization or by the interaction of the laser-induced plasma with solid targets. Previous studies have shown that the removed materials are in monomer form in the beginning stage, and then interact with each other and ions contained in the plasma clouds to form very small clusters (Wood *et al*., 1998). Coagulation or coalescence of these clusters forms primary particles, with sizes within a range of a few nanometers (Kawakami *et al*., 1999; Ogawa *et al*., 2002; Ullmann *et al*., 2002). Further collisions among these primary particles finally generate aggregates, which are typically tens of nanometers or larger (Friedlander *et al*., 1998; Ogawa *et al*., 2002). This technique has been considered an effective and convenient method for surface decontamination and cleaning (Schmidt *et al*., 2001; Li, 2002; Minami *et al*., 2002), as well as for nanoparticle generation (Kawakami *et al*., 1999; Ogawa *et al*., 2002; Ullmann *et al*., 2002). However, many unknowns remain.

As a surface cleaning technique, laser ablation is used for decontamination and decommissioning (D&D) of a large number of nuclear facilities at U.S. Department of Energy (DOE) complexes across the United States. However, the large amount of small particles produced in the process could contain contaminants, such as toxic heavy metals (e.g., Cr, Hg, Pb, and Ni), radionuclides (e.g., Th, Cs, and U), and hazardous organic solvents. These particles lead to secondary pollution and may cause adverse health effects on humans. Hence, it is necessary to characterize the particles generated in the process of different laser operations.

Previous studies on the characterization of nanoparticles produced in laser decontamination processes used a SMPS system (Lee and Cheng, 2004a, b). The laboratory-prepared target surfaces were made from Portland cement (cement) with or without a toxic heavy metal, chromium (Cr); stainless steel 316; and pure alumina. Particle size and number concentration were characterized with respect to laser energy, wavelength, and the type of target materials. However, the long DMA (TSI model 3081) used in their SMPS system has very low particle transmission efficiency when characterizing particles with diameters smaller than 20 nm. Further, the use of an ultrafine condensation particle counter (UCPC, TSI model 3025A) limited the maximal number concentration to 10^5 #/cm^3. In this article, we report the experimental results of nanoparticle characterization using a Fast-Scanning Electrical Nanoparticle Sizer (FSENS, previously named as nASA, Han *et al*., 2000) under the same experimental conditions as those in previous studies (Lee and Cheng, 2004a, b).

EXPERIMENTAL OVERVIEW

Sample materials and experimental setup

Cement, chromium-embedded cement, stainless steel, and alumina target materials were used in this experiment. Cement and stainless steel are commonly used in DOE installations. Chromium-embedded cement was used to examine how chromium, one of the contaminants of concern, affects the characteristics of particles generated during laser ablation. Alumina (Al_2O_3) was used as a comparison material because it is a comparatively pure substance, which has very favorable surface properties for studies of laser ablation (Chase, 1994). The method for preparing the target surfaces and the chemical compositions of the target materials have been reported by Lee and Cheng (2004a, b).

Fig. 1 shows the laser ablation experimental setup. It is identical to the one used by Lee and Cheng (2004b) except that FSENS was used for particle size distribution measurement, instead of SMPS. An Nd:YAG laser (Newwave Research, Model INDI-10) was used as the energy source, from which three wavelengths (266-nm, 532-nm, 1064-nm) can be emitted. A small part of the laser beam was split to an energy meter (Molectron EM 500 Single-Channel Joulemeter), by which the laser energy was monitored. The major part of the laser beam was passed through a focusing lens to achieve much higher fluence, enough to produce plasma around the target surfaces, and consequently generate a large number of nanoparticles. The aerosol stream was sampled from the laser ablation chamber and characterized by FSENS. The operation and properties of the laser beam applied in the experiment have been described in detail by Lee and Cheng (2004b).

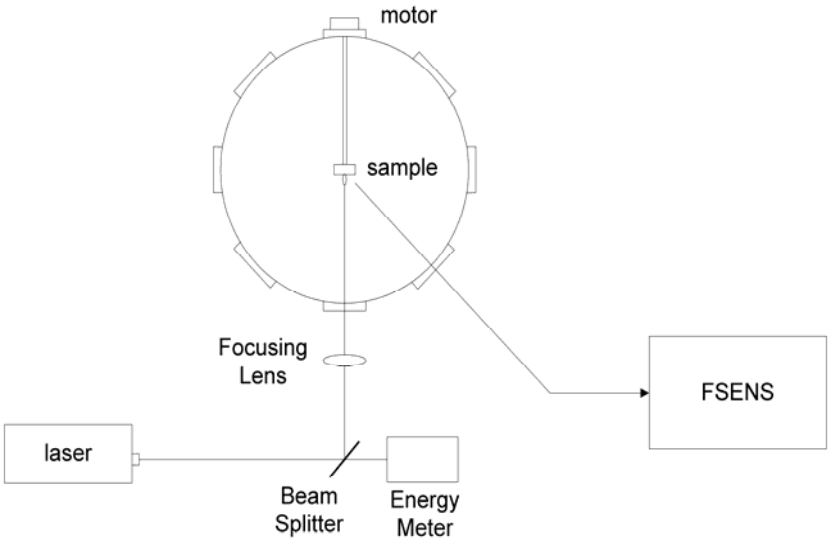

Fig. 1. Experimental setup for characterizing nanoparticles generated from laser decontamination.

For each fluence applied to a material surface at all three wavelengths, at least 20 measurements were made to make sure that the particle size distributions reached the final state. The FSENS data acquisition software was used to process the data and generate ASCII files, which were further analyzed in DISFIT (Chimera Technologies, Inc., 2004) to characterize the measured size distributions.

Fast-scanning electrical nanoparticle sizer (FSENS)

The FSENS (Fast-Scanning Electrical Nanoparticle Sizer), an upgraded model of the nASA (nanometer aerosol size analyzer, Han *et al*., 2000), was constructed and used in this experiment to characterize the size distributions of particles in high concentration. The measurement cycling time of the FSENS is 1 s (compared with 135 s for a commercial SMPS system). Fig. 2 is a schematic diagram of the sizer, consisting of a Po^{210} bipolar aerosol charger, a Nano-DMA column for particle sizing (Chen *et al*., 1998), and an aerosol electrometer (TSI model 306802) as the particle counter. Compared with the prototype model (nASA), the latest sizer is fully computer-controlled, including the recirculation flowrate between sheath and excess flow ports for Nano-DMA, in addition to the voltage control (set-and-readback control loop) and electrometer readout acquisition.

A solid-state, high-voltage power supply was added to the sizer to reduce its voltage scanning time. The Labview software for controlling the Nano-DMA sheath flowrates, voltage scanning scheme, data acquisition, and on-line data reduction scheme was improved to ensure fast data display and reliable operation of the FSENS. The Nano-DMA in this sizer can measure nanoparticles in the size range of 2-100 nm. The use of an aerosol electrometer as the particle counter allows it to measure particles in concentrations exceeding the limit of an Ultrafine CPC. The nASA arrangement greatly reduces the need for high dilution of the sampled aerosol stream and reduces the measurement cycling time to 3 s (compared with 135 s for a typical SMPS). FSENS further reduces the voltage scan time to 1 s by the use of solid-state high voltage power supply instead of that used in nASA.

In the experiment, the aerosol flow and sheath flow were operated at 2.2 L/min and 8.5 L/min, respectively, and particles in diameters ranging from 2-85 nm were measured. Despite the FSENS's capability of detecting particles in diameters less than 5 nm, very low charged particle counts were detected during the experiment for particles less than 6 nm in size. This is because of the low charging efficiency of the FSENS bipolar aerosol charger for particles less than 5 nm in diameter. The low concentration of charged particles results in a low electrical current detected by aerosol electrometer. Due to low signal-to-noise ratio, detection of such low currents usually requires a longer time than that in the FSENS scanning mode operation used in this study. Consequently, we have limited the lower size particle size distributions presented here to 6 nm. Note that the 2.2 L/min aerosol flow, higher than that used by SMPS (typically less than 1.5

L/min), was used by FSENS. The increased aerosol flowrate used by FSENS improves the chance of detecting charged particles at low concentration.

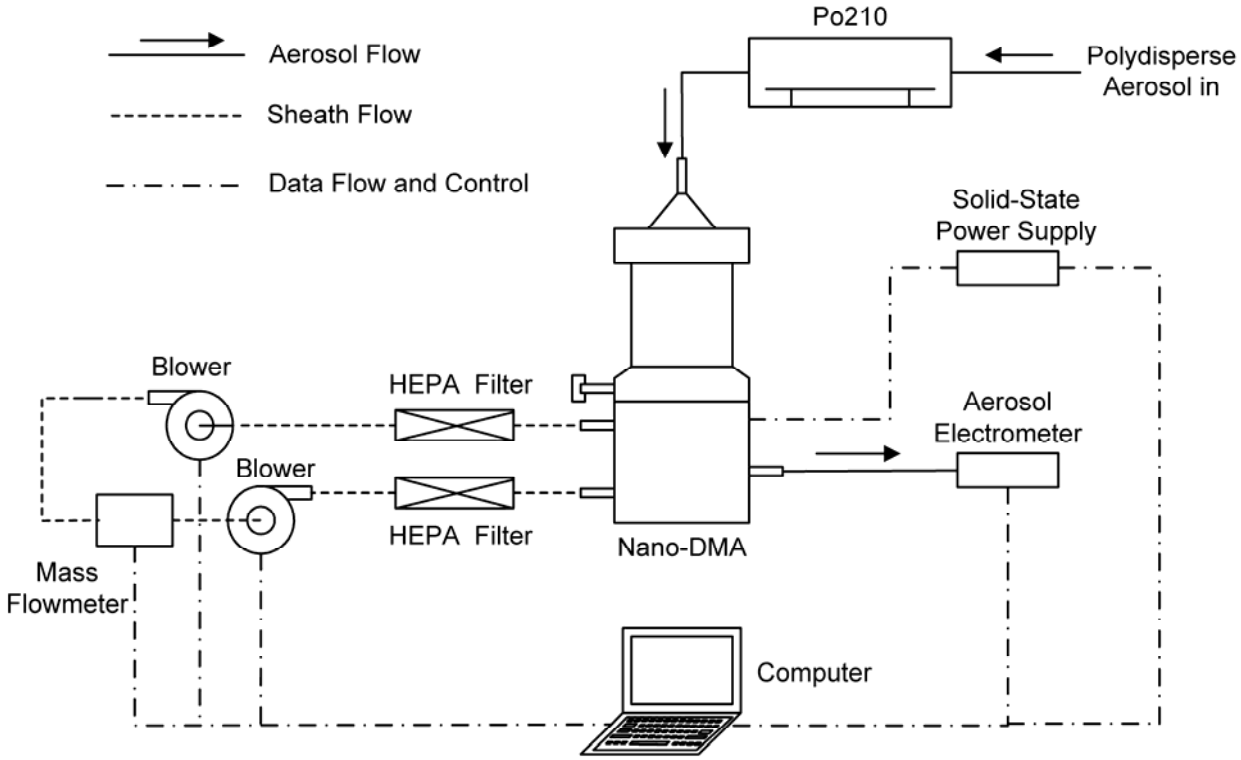

Fig. 2. Schematic diagram of the Fast-Scanning Electrical Nanoparticle Sizer (FSENS).

RESULTS AND DISCUSSION

Bimodal particle size distributions

Bimodal particle size distributions were observed for all the experimental runs. DISFIT (Chimera Technologies, Inc., 2004) software was used for curve fitting of the measured size distribution data. It was found that the bimodal size distribution, with the first mode (the smaller particle size peak) fitted by a lognormal distribution and the second mode (the larger particle size peak) fitted by a Rosin-Rammler distribution, was best suited all the collected data. Fig. 3 shows three examples of measured size distributions and their corresponding curve fittings. The χ^2 for this curve fitting of all the example data was 4.43×10^{-3}, indicating good curve fittings of the measured size distributions. From the fitted size distributions, we determined the number concentrations of both modes (N_1 and N_2), the geometric mean diameter of both modes (d_{g1} and d_{g2}), and the geometric standard deviation of both modes (σ_{g1} and σ_{g2}) for each experimental condition.

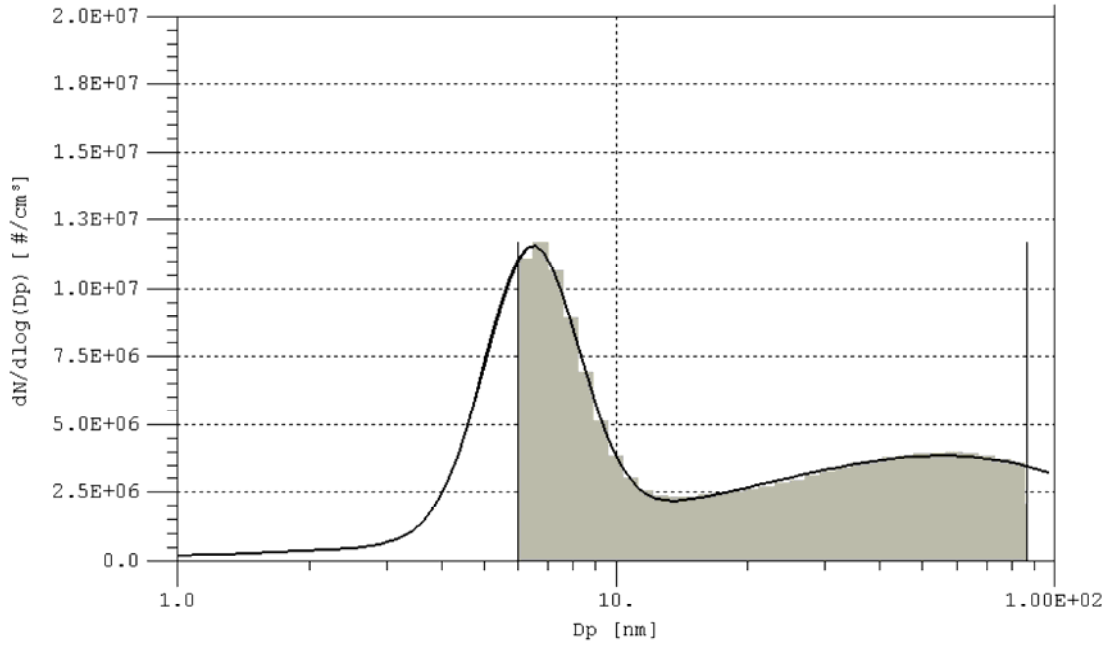

Fig. 3(a). Particle size distribution and DISFIT curve fitting for particles generated (a) from a stainless steel target with a laser of 266-nm wavelength and 324 J/cm^2 fluence.

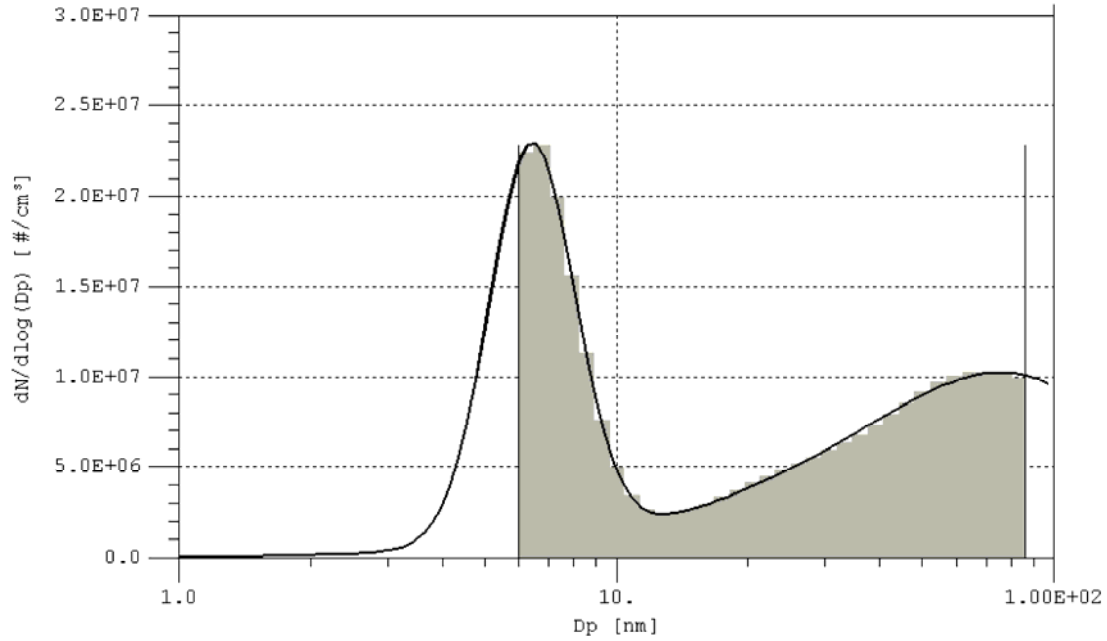

Fig. 3(b). Particle size distribution and DISFIT curve fitting for particles generated (b) from a cement target with a laser of 532-nm wavelength and 562 J/cm^2 fluence.

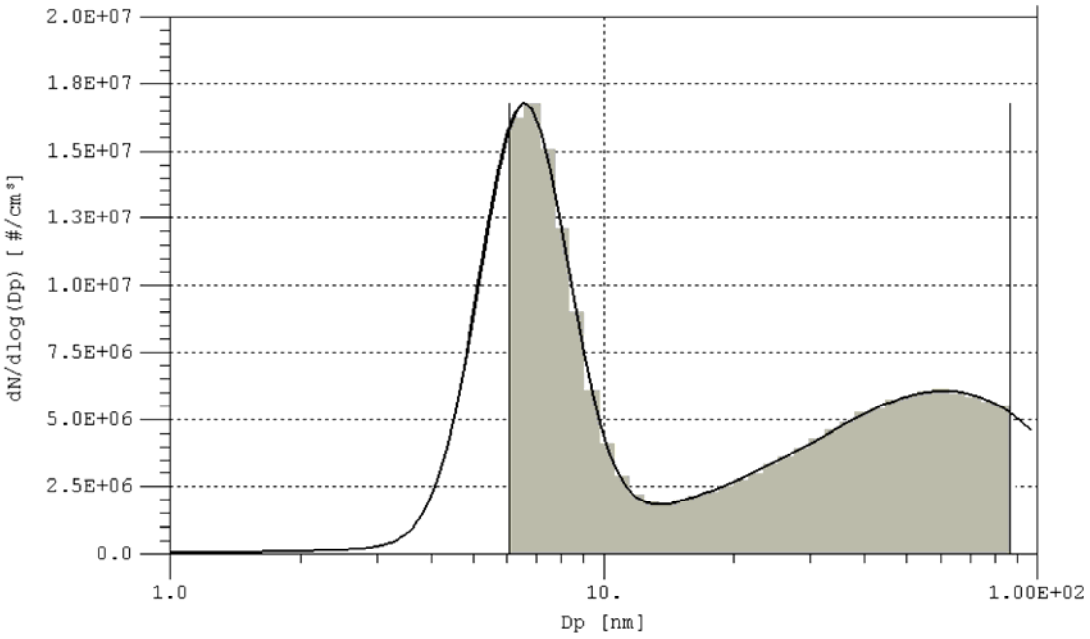

Fig. 3(c). Particle size distribution and DISFIT curve fitting for particles generated (c) from a chromium-embedded cement target with a laser of 1064-nm wavelength and 1180 J/cm^2 fluence.

For all the experimental cases, the geometric mean diameters of the 1st mode (d_{g1}) are in a very narrow size range (around 5.7-6.6 nm) with σ_{g1} varying from 1.225-1.379. These small particles might be primary ones formed directly by the nucleation, and could be described as the nucleation mode. The observation that the primary particle size varies very little for different materials and laser conditions is consistent with the observations by Ullmann *et al*. (2002). However, the nucleation mode was not observed in the SMPS data (Lee and Cheng, 2004b). The real reason for the discrepancy is unknown to the authors. The authors had done comprehensive calibration on the response of FSENS both in steady and dynamic conditions. The proper responses from FSENS indicate no instrumentation error. The possible reason for the mode not being detected by SMPS is that serious losses for particles smaller than 10 nm may have been encountered in both impactor and long DMA used in SMPS. The situation may have further worsened with the reduced aerosol flowrate and low charging efficiency of bipolar aerosol charger used in SMPS.

The geometric mean diameters of the 2nd mode (d_{g2}) are in the range of tens of nanometers, which could represent aggregates formed by the collision of the primary particles (Friedlander *et al*., 1999; Ogawa *et al*., 2002). The 2nd mode can be referred as the coagulation mode.

Particle size of the coagulation mode of steady-state size distribution

As described in Experimental Overview, at least 20 measurements were made for each experimental condition to ensure that the particle size distributions in the final state were measured. For each run at least three measured final-state size distributions were selected and analyzed in the curve-fitting process. For some cases with low laser fluence, no size distribution data could be selected for the curve fitting, because the peak in the coagulation mode was not distinctive. These data were excluded from the analysis.

As shown in Fig. 4(a), for the 266-nm wavelength, the geometric mean diameters of the coagulation mode change very little (77-90 nm) with the laser energy for all materials, except for the stainless steel sample. Statistical t-tests performed by Lee and Cheng (2004b) with SMPS data also suggested that the geometric mean diameters of particles produced from the same materials are statistically identical irrespective of laser fluence. For the stainless steel, the geometric mean diameter of the coagulation mode increases as the laser fluence increases (from 38-56 nm with fluence from 6.6-32 J/cm^2).

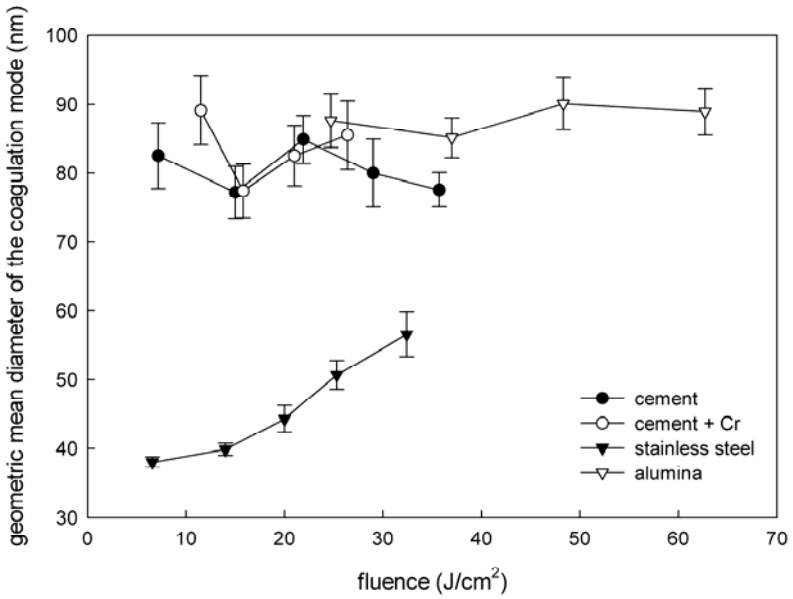

Fig. 4(a). Geometric mean diameters in the coagulation mode for particles generated from different materials (a) by a laser of 266-nm wavelength.

Fig. 4(b) shows the results for the 532-nm wavelength laser. For the case of stainless steel, a broad size distribution without an obvious peak in the coagulation mode was observed for all the energy levels. The data was thus not included in the plot. For the other three materials, there was also no obvious trend between the geometric mean diameter of the coagulation mode and the laser fluence. This finding is consistent with the observations of Lee and Cheng (2004b). Figs.

4(a) and (b) indicate that the geometric mean diameters of the coagulation mode for different materials are very different for the 532-nm laser, and they also differ from those produced by the 266-nm laser. Particles produced from the alumina sample had a much smaller geometric mean diameter of the coagulation mode for the 532-nm laser.

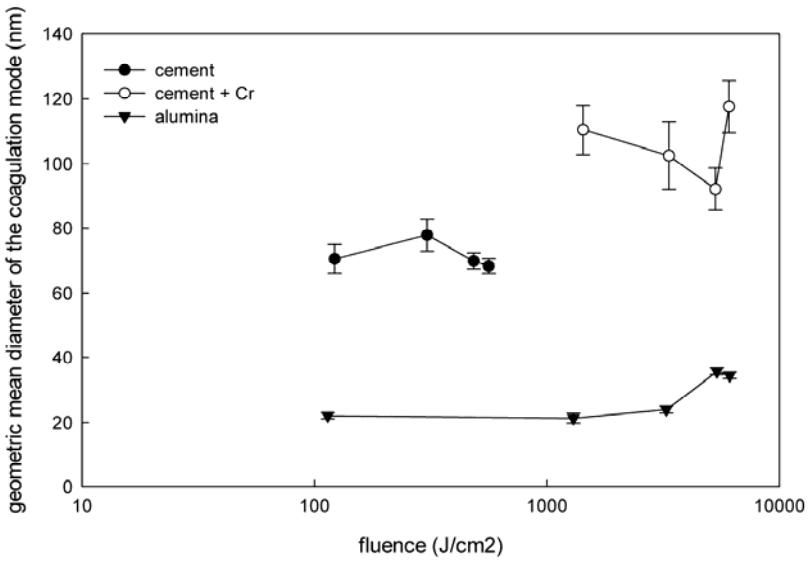

Fig. 4(b). Geometric mean diameters in the coagulation mode for particles generated from different materials (b) by a laser of 532-nm wavelength.

The results for the 1064-nm laser are shown in Fig. 4(c). Again, the geometric mean diameter of the coagulation mode of the same material does not change much with laser energy, except for stainless steel. For the stainless steel, the geometric mean diameter of the coagulation mode increases from 40-68 nm with laser fluence increasing from 23-52 J/cm^2, and then changes little with further increases in laser fluence. The result for the cement samples is very different from those for the other three materials at this wavelength. Compared with those for the 266- and 532-nm laser, the observations for the 1064-nm laser are also quite different.

It is thus concluded that the geometric mean diameter of the coagulation mode changes very little with laser energy for a given material under a certain wavelength laser, and the differences in geometric mean diameter of the coagulation mode among different materials and wavelengths are very obvious. This finding might reflect different particle aggregation processes for different materials and lasers of different wavelengths. Further, the laser energy had little effect on the particles' aggregation process after reaching a certain level.

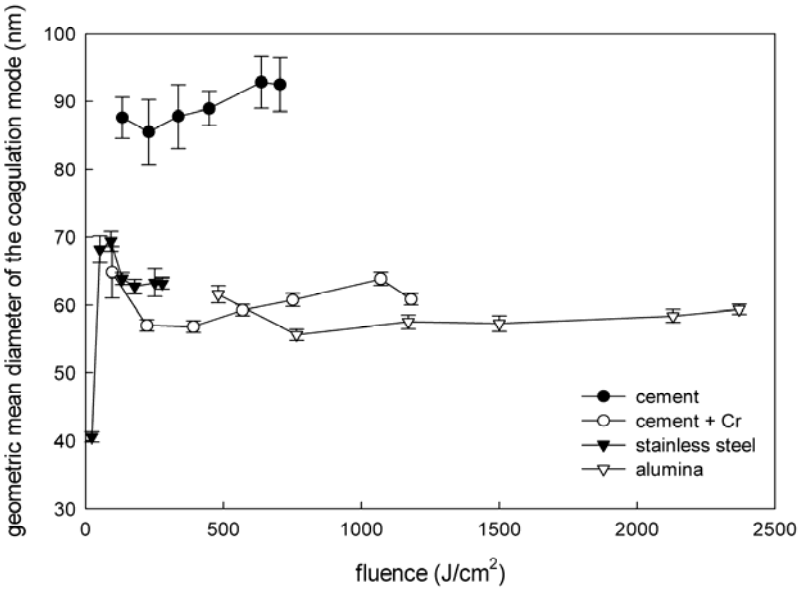

Fig. 4(c). Geometric mean diameters in the coagulation mode for particles generated from different materials by a laser of 1064-nm wavelength.

Particle production at final state

From the DISFIT curve fittings, the total number concentrations of both modes were calculated. It is worth mentioning that the total number concentration given here is not the number summation of particles in all the measured size channels. It is the value calculated from the fitted size distribution function. Fig. 5 shows the total number concentration of particles produced by 266-, 532-, and 1061-nm lasers in the 1st mode. Figure 6 shows the same data for the coagulation mode. For the 1st mode the coefficients of variation among the experimental runs for 266-, 532-, and 1061-nm lasers were 3.62-8.65%, 1.27-6.04%, and 1.64-5.29%, respectively. For the coagulation mode the corresponding coefficients were 3.19-7.79%, 2.50-9.84%, and 1.60-5.11% for 266-, 532- and 1061-nm lasers, respectively.

Comparing Fig. 5 with Fig. 6, we found that the total number concentrations of particles produced from the same wavelength laser have similar trends in the nucleation and coagulation modes. The relationship between the particle concentration and fluence appears to be parabolic for all the cases. Regression lines are also given in each figure. The correlation, R^2, was greater than 0.99 for all the cases of the 266-nm laser, $\geq$ 0.98 for the 532-nm laser, and $\geq$ 0.94 for any case of the 1064-nm laser. This parabolic trend for each material under lasers of different wavelengths is very similar to those obtained in SMPS measurements by Lee and Cheng (2004b).

Among all samples, the stainless steel sample produced the highest particle number concentration at a given fluence for 532- and 1064-nm lasers. Alumina produced the lowest particle number concentration at a given fluence for 266- and 1064-nm lasers. The absorption

coefficient of laser energy for stainless steel is larger than that for alumina, which might well explain the finding. Further, the production of particles from cement samples was greatly inhibited by embedded chromium under 532- and 1064-nm laser ablation, although with the 266-nm laser, chromium had almost no effect on particle production.

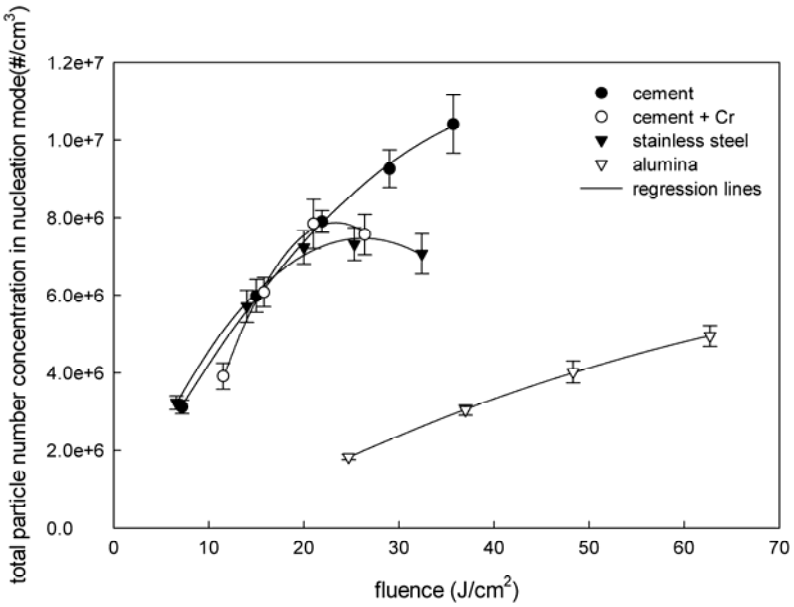

Fig. 5(a). Observed parabolic relationship between the total generated number concentration (#/cm^3) in the nucleation mode and (a) the 266-nm wavelength laser fluence (J/cm^2).

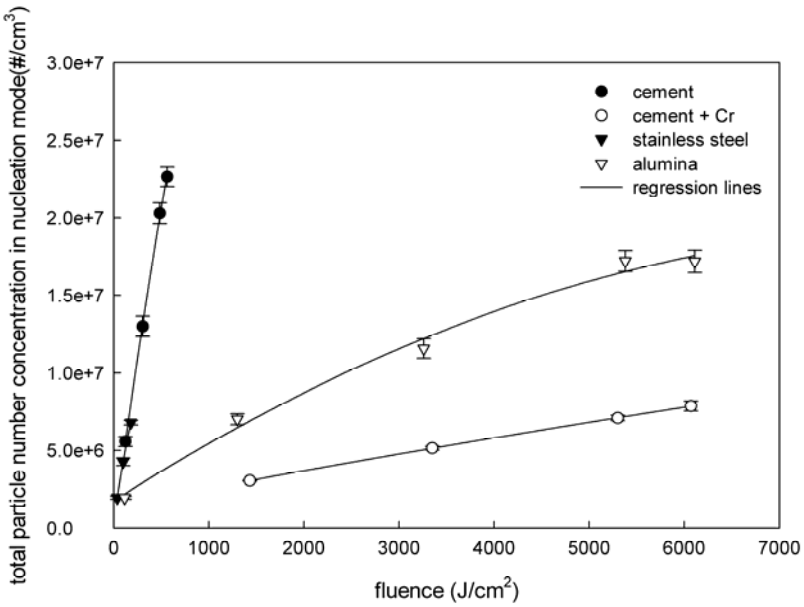

Fig. 5(b). Observed parabolic relationship between the total generated number concentration (#/cm^3) in the nucleation mode and (b) the 532-nm wavelength laser fluence (J/cm^2).

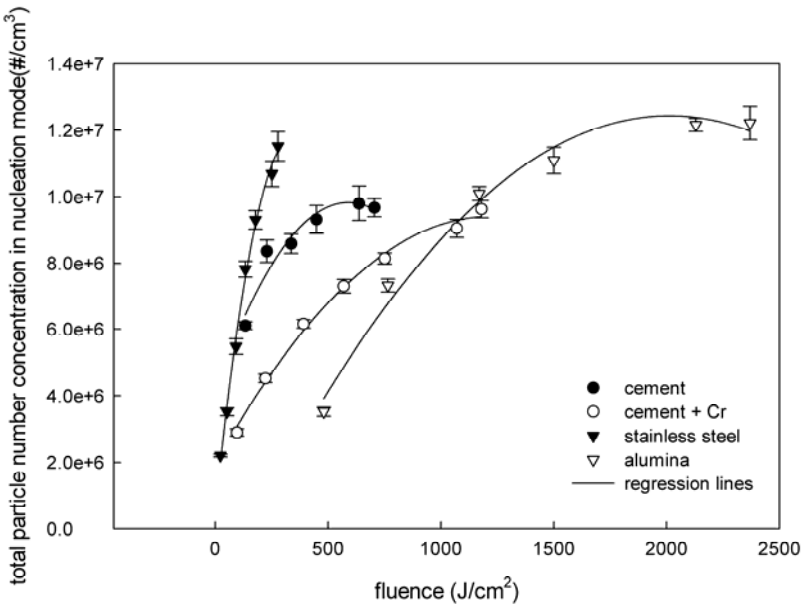

Fig. 5(c). Observed parabolic relationship between the total generated number concentration (#/cm^3) in the nucleation mode and (c) the 1064-nm wavelength laser fluence (J/cm^2).

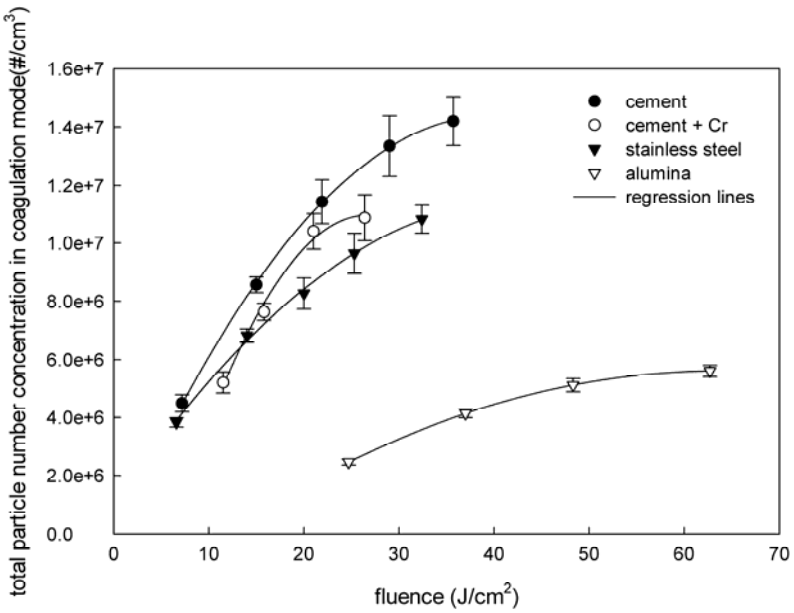

Fig. 6(a). Observed parabolic relationship between the total generated number concentration (#/cm^3) in the coagulation mode and (a) the 266-nm wavelength laser fluence (J/cm^2).

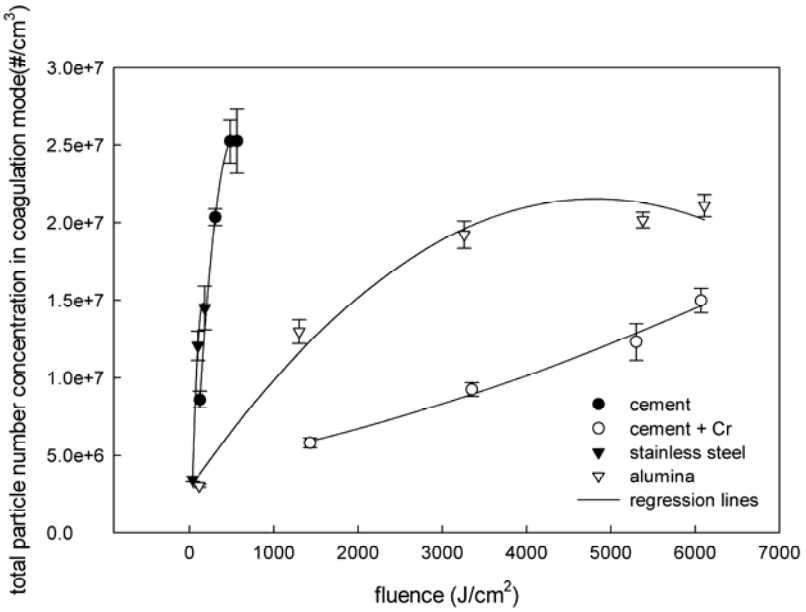

Fig. 6(b). Observed parabolic relationship between the total generated number concentration (#/cm^3) in the coagulation mode and (b) the 532-nm wavelength laser fluence (J/cm^2).

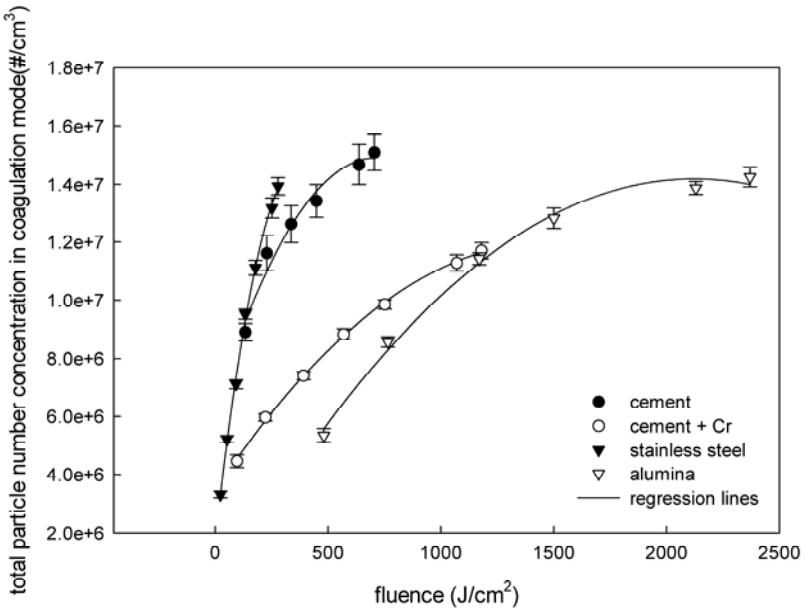

Fig. 6(c). Observed parabolic relationship between the total generated number concentration (#/cm^3) in the coagulation mode and (c) the 1064-nm wavelength laser fluence (J/cm^2).

Nanoparticle dynamics at low laser fluence

The fast voltage-scan feature of FSENS makes it possible to get snapshots of nanoparticle dynamics during laser ablation under low laser fluence. Lower laser fluence produces lower particle concentration, and consequently it takes longer for primary particles to coagulate and mature into the final bimodal size distributions than in cases of high particle concentration. Fig. 7

shows the nanoparticle dynamics for stainless steel in the 1064-nm laser ablation process with fluence of 23 J/cm^2.

Fig. 7 shows that during the laser ablation process the nucleation mode (i.e., primary particles) was first produced, and then the coagulation mode was formed gradually by aggregation. The peak size of the coagulation mode obviously moves to the larger particle size range with increased laser ablation time. The growth process stops when the size distribution at the mature state has been reached. The collected size distributions well reflect the nanoparticle dynamics, and could be used in future study on the modeling of particle formation during laser ablation process.

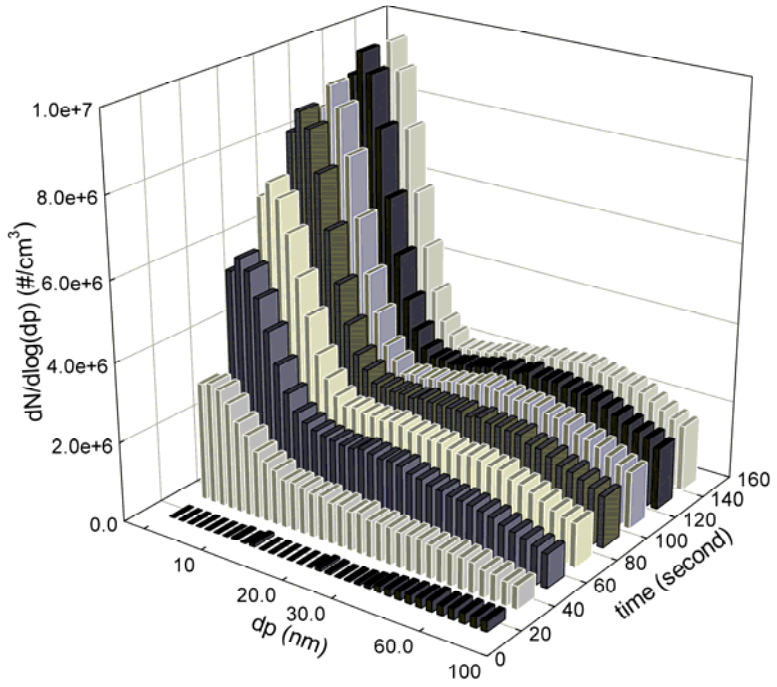

Fig. 7. Snapshots of nanoparticle dynamics in laser ablation by FSENS measurement (Target Material: Stainless Steel; Laser Wavelength: 1064 nm; Laser Fluence: 23 J/cm^2).

CONCLUSIONS

FSENS, with the ability to measure high concentration particle size distributions in a 2-100 nm size range, and with a measuring cycling time less than 3 s, was used to investigate nanoparticles generated under different operational conditions in laser ablation. Sample materials used in this study were cement, chromium-embedded cement, stainless steel, and alumina. Different from published SMPS data under the same experimental condition (Lee and Cheng, 2004), a bimodal size distribution, with the nucleation mode changing very little in geometric mean diameter (5.7-

6.6 nm) and geometric standard deviation (1.225-1.379), was observed for all the experimental and laser cases. The two modes in measured size distributions possibly represent primary particles in the nucleation mode (i.e., smaller size peak) and aggregates in the coagulation mode (i.e., larger size peak). The primary particle size varies very little for different material and laser condition, consistent with the observation by Ullmann *et al*. (2002). The geometric mean diameter of the coagulation mode varied little with laser energy for a given material and laser wavelength. However, the difference in the geometric mean diameter of the coagulation mode among different materials and wavelengths is very obvious, probably resulting from different particle aggregation/condensation processes for different materials and laser wavelengths. The observations for the coagulation mode at the final state are consistent with those obtained from SMPS measurement by Lee and Cheng (2004b). Further study will be needed to investigate the aggregation/condensation process for different materials and lasers with different wavelength.

Finally, this study demonstrates that with the fast voltage scanning feature of FSENS it is possible to get snapshots of the nanoparticle dynamics in laser ablation at low fluence. At low fluence, the low particle number concentration produced in the laser ablation process requires a longer time to develop steady-state particle size distributions. Under this condition the FSENS is able to obtain snapshots of the particle formulation process. The collected information will be very useful in the modeling study of nanoparticle formulation in laser ablation.

ACKNOWLEDGEMENTS

The authors are grateful for the support partially provided by the Department of Energy Office of Science Office of Biological and Environmental Research Management Science Program (EMSP) under Project number 82,807. The Oak Ridge National Laboratory is managed by UT-Battelle, LLC, for the U. S. Department of Energy under contract DE-AC05-00OR22725.

REFERENCES

Chase, L.L. (1994). *Laser Ablation and Optical Surface Damage.* J.C. Miller (Ed.), Laser Ablation: Principles and Applications, Springer Series in Materials Science: Vol. 28, pp. 53-84. NY: Springer.

Chen, D.R., Pui, D.Y.H., Hummes, D., Fissan, H., Quant, F.R. and Sem, G.J. (1998). Design and Evaluation of a Nanometer Aerosol Differential Mobility Analyzer (Nano-DMA). *J. Aerosol Sci.* for the Special Issue on Nanometer Particles, 29: 497.

Friedlander, S.K., Jang, H.D. and Ryu, K.H. (1998). Elastic Behavior of Nanoparticle Chain Aggregates. *Appl. Phys. Lett.* 72: 173.

Han, H.S., Chen, D.R., Pui, D.Y.H. and Anderson, B.E. (2000). A Nanometer Aerosol Size Analyzer (nASA) for Rapid Measurement of High-Concentration Size Distributions. *J. Nanopart. Res.* 2: 43.

Kawakami, Y., Seto, T. and Ozawa, E. (1999). Characteristics of Ultrafine Tungsten Particles Produced by Nd:YAG Laser Irradiation. Applied Physics A (Suppl., S249).

Lee, D.-W., Cheng, M.-D. (2004a). Investigations of Nanoparticle Generation During Surface Decontamination by Laser Ablation at Low Fluence. *J. Aerosol Sci.* 35: 1513.

Lee, D.-W., Cheng, M.-D. (2004b). Particle Generation by Laser Ablation During Surface Decontamination. *J. Aerosol Sci.* 35: 1527.

Li, L. (2002). The Potential Role of High-Power Lasers in Nuclear Decommissioning. *Nuclear Energy-Journal of British Nuclear Energy Society,* 41: 397.

Minami, K., Lawrence, J., Li, L., Edwards, R.E. and Gale, A.W. (2002). Comparison of CO_2, Nd:YAG and High Power Diode Lasers for the Ablation of Tile Grout. *Appl. Surf. Sci.* 186: 256.

Ogawa, K., Vogt, T., Ullmann, M., Johnson, S. and Friedlander, S.K. (2002). Elastic Properties of Nanoparticle Chain Aggregates of TiO_2, Al_2O_3, and Fe_2O_3 Generated by Laser Ablation. *J. Appl. Phys.* 87: 63.

Schmidt, M.J.J., Li, L. and Spencer, J.T. (2001). Removal of Chlorinated Rubber Coatings from Cement Surfaces Using an RF Excited CO_2 Laser. *J. Mater. Process. Technol.* 114: 139.

Ullmann, M., Friedlander, S.K. and Schmidt-Ott, A. (2002). Nanoparticle Formation by Laser Ablation. *J. Nanopart. Res.* 4: 499.

Wood, R.R., Leboeuf, J.N., Chen, K.R., Geohegan, D.B. and Puretzky, A.A. (1998). Dynamics of Plume Propagation, Splitting, and Nanoparticle Formation During Pulsed-Laser Ablation. *Appl. Surf. Sci.* 151: 127-9.

Received for review, September 21, 2006
Accepted, January 4, 2007